Journal of Materials Chemistry A



PAPER

View Article Online
View Journal | View Issue



Cite this: *J. Mater. Chem. A*, 2022, **10**, 1940

Enhancing the propylene/propane separation performances of ZIF-8 membranes by post-synthetic surface polymerization†

Sunghwan Park,^a Kie Yong Cho^b and Hae-Kwon Jeong (1)**ac

Zeolitic-imidazole framework-8 (ZIF-8) membranes have shown exceptional propylene/propane separation performances. Their commercial applications have, however, been impeded by several challenges. One such challenge is the difficulty of managing microstructural defects (*i.e.*, grain boundary defects) in a consistent manner, leading to poor membrane performances and ultimately to a reproducibility issue. Herein, we introduce a new effective strategy to seal the microstructural defects of polycrystalline ZIF-8 membranes using post-synthetic surface polymerization which consists of two steps: (1) introduction of initiator ligands on the membrane surface by post-synthetic ligand exchange and (2) *in situ* polymerization of poly(methyl methacrylate) (PMMA) *via* atom transfer radical polymerization. The ZIF-8 membranes were fully covered with ultra-thin PMMA layers of sub-10 nm thickness, increasing the propylene/propane separation factor from ~60 to ~106 with unexpectedly increased propylene permeance, effectively improving the membrane reproducibility. The enhanced separation properties of the PMMA-coated ZIF-8 membranes were attributed to the ultra-thin PMMA layers as well as to the possible facilitated propylene transport by Cu ions in the PMMA layers.

Received 8th October 2021 Accepted 15th December 2021

DOI: 10.1039/d1ta08705c

rsc.li/materials-a

Introduction

ZIF-8 consists of Zn^{2+} metal nodes tetrahedrally coordinated with 2-methylimidazole (2-mIm) linkers, forming a sodalite (SOD) topology. The effective aperture size of the six-membered ring in ZIF-8 was estimated to be 4.0–4.2 Å, much larger than its crystallographically defined one of 3.4 Å due to the swing motion of the organic linkers, thereby being suitable for propylene/propane (C_3H_6/C_3H_8) separation.² As such, polycrystalline ZIF-8 membranes have shown exceptionally high C_3H_6/C_3H_8 separation performances.³

Despite their great potential, the practical application of ZIF-8 membranes for industrial gas separation faces several issues.⁴ One such issue has to do with the reproducibility of consistent-quality membranes. As inherent to any polycrystalline membranes such as zeolite membranes, polycrystalline ZIF-8 membranes contain non-selective microstructural grain boundaries (*i.e.*, microscopic defects) that compromise their separation performances. It is, however, often difficult to obtain

Polydimethylsiloxane (PDMS) has been widely used as a coating material to improve the grain boundary structures of polycrystalline membranes because it is highly gas permeable, inexpensive, and easily processible. Sheng et al. 10 reported that when coated with PDMS, poorly intergrown defective ZIF-8 membranes showed a significantly improved C₃H₆/C₃H₈ separation factor which was attributed to the effectively blocked defects and the hindered flexibility of ZIF-8 upon PDMS coating.10 Other polymers (both rubbery and glassy) such as Pebax®, PTMSP (poly[1-(trimethylsilyl)-1-propyne]), PIM-1 (polymers of intrinsic microporosity-1), and Matrimid® have also been used to seal the microscopic defects of polycrystalline membranes. 10-12 However, defect sealing with a polymer often leads to a substantial decrease in the gas permeance (i.e., flux) of the polycrystalline membranes, which is not desirable for their practical gas separation applications. This undesirable decrease in the permeance of the coated polycrystalline membranes is because of the limitation of the conventional solution processing that leads to undesirably thick polymer

polycrystalline membranes with consistent grain boundary structures that depend greatly on processing conditions,^{5,6} consequently giving rise to a reproducibility issue. In this regard, the post-synthetic surface coating of polycrystalline membranes is a practical strategy to enhance the reproducibility of polycrystalline ZIF and MOF membranes by effectively improving their grain boundary structures (*i.e.*, sealing microscopic defects).⁷⁻¹² It is noted that the surface coating strategy has been successfully applied to commercial polymer membranes.¹³

[&]quot;Artie McFerrin Department of Chemical Engineering, Texas A&M University, 3122 TAMU, College Station, TX 77843-3122, USA. E-mail: hjeong7@tamu.edu

^bDepartment of Industrial Chemistry, Pukyong National University, 45 Yongso-ro, Nam-gu, Busan 48513, Republic of Korea

Department of Materials Science and Engineering, Texas A&M University, 3122 TAMU, College Station, TX 77843-3122, USA

[†] Electronic supplementary information (ESI) available. See DOI: 10.1039/d1ta08705c

coating layers (i.e. >100 nm). It is, therefore, highly desirable to develop a new coating strategy to efficiently seal the grain boundary defects of polycrystalline membranes ideally without compromising the flux of the membranes.

Post-synthetic ligand exchange (PSLE) (also known as solvent-assisted ligand exchange (SALE)14) has been successfully used in MOFs to modify surface properties,15 to introduce functional groups,16 to obtain particular morphologies,17 to reduce membrane thicknesses,18 to tune effective aperture sizes,19 etc. Recently, Cohen and coworkers20 reported freestanding ZIF-8 films by self-assembling ZIF-8 nanoparticles that were modified by PSLE and subsequently polymerized by atomic transfer radical polymerization (ATRP). The thin poly(methyl methacrylate) (PMMA) layer grown on ZIF-8 surfaces enabled the formation of a free-standing self-assembled ZIF-8 monolayer.

In this study, we report a new defect sealing strategy based on Cohen's post-synthetic surface polymerization (i.e., PSLE

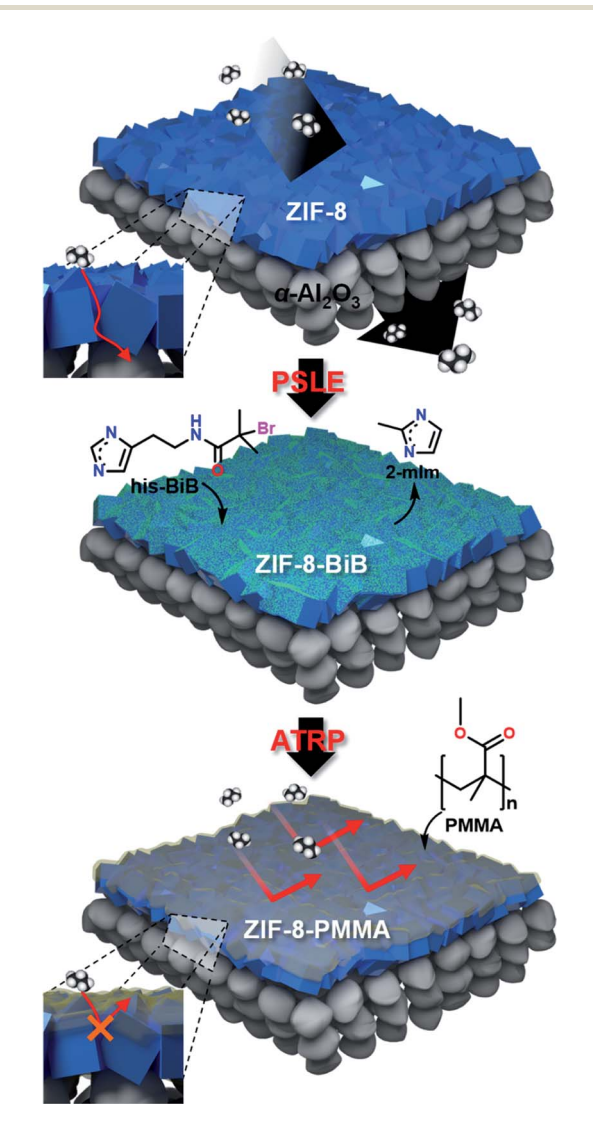


Fig. 1 Schematic illustration of the defect sealing of a ZIF-8 membrane via post-synthetic ligand exchange (PSLE) followed by atom transfer radical polymerization (ATRP).

followed by ATRP) to seal the grain boundary defects of polycrystalline ZIF-8 membranes. The new strategy led to the formation of an ultra-thin PMMA layer polymerized on ZIF-8 membranes. Each step of the post-synthetic surface polymerization process was systematically investigated. The physical and gas separation properties of the resulting membranes were thoroughly characterized.

Results and discussion

Fig. 1 illustrates the procedure of the defect sealing of a ZIF-8 membrane using post-synthetic surface polymerization (hereafter PSSP) consisting of PSLE and subsequent ATRP. The PSLE modifies the surface of the ZIF-8 membrane with his-BiB by replacing 2-mIm (ZIF-8 linker), resulting in a ZIF-8-BiB membrane. Considering the effective aperture size of ZIF-8 (i.e., 4.0–4.2 Å) and the kinetic diameter of his-BiB (i.e., \sim 6.6 Å), it is likely that his-BiB replaces the 2-mIm close to the surface of ZIF-8 (i.e., diffusion-limited).21 Since polycrystalline ZIF-8 membranes exhibit grain boundary defects on the scale of \sim 1–2 nm, ^{5,22} larger than his-BiB, the grain boundary surfaces are likely exchanged with his-BiB as well along with the external surfaces. It is noted that the bromide of his-BiB initiates ATRP to grow PMMA on the surface (both the grain boundary surface and the external surface) of the membrane. The PMMA polymerized in situ on the ZIF-8-BiB membrane is expected to effectively seal the grain boundaries, thereby preventing gas molecules from bypassing and consequently enhancing the separation factor of the ZIF-8 membrane. Furthermore, due to the limited amount of the initiator (his-BiB), polymerization is limited to the top surface of the membrane, thereby forming an ultra-thin PMMA layer with a uniform thickness which ensures the preservation of the gas permeance of the ZIF-8 membrane.20,23

Fig. 2 presents the PXRD diffraction patterns of a ZIF-8 seed layer after microwave seeding and the corresponding ZIF-8 membrane after secondary growth. Both of the diffraction

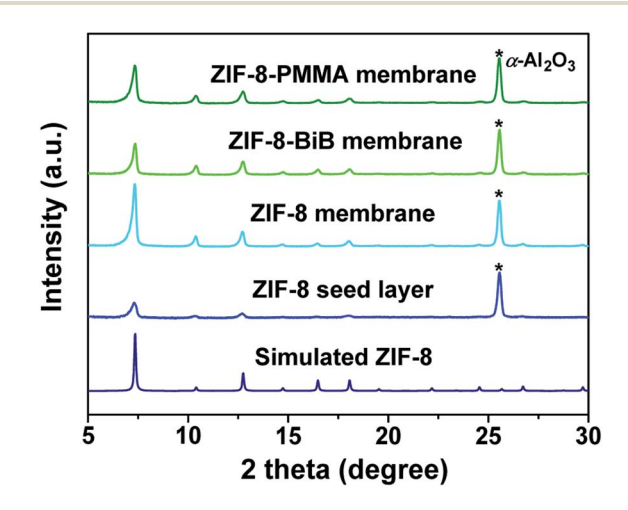


Fig. 2 PXRD patterns of a ZIF-8 seed layer after microwave seeding, a ZIF-8 membrane after secondary growth, a ZIF-8-BiB membrane after PSLE, and a ZIF-8-PMMA membrane after ARTP. The simulated ZIF-8 pattern is included as a reference.1

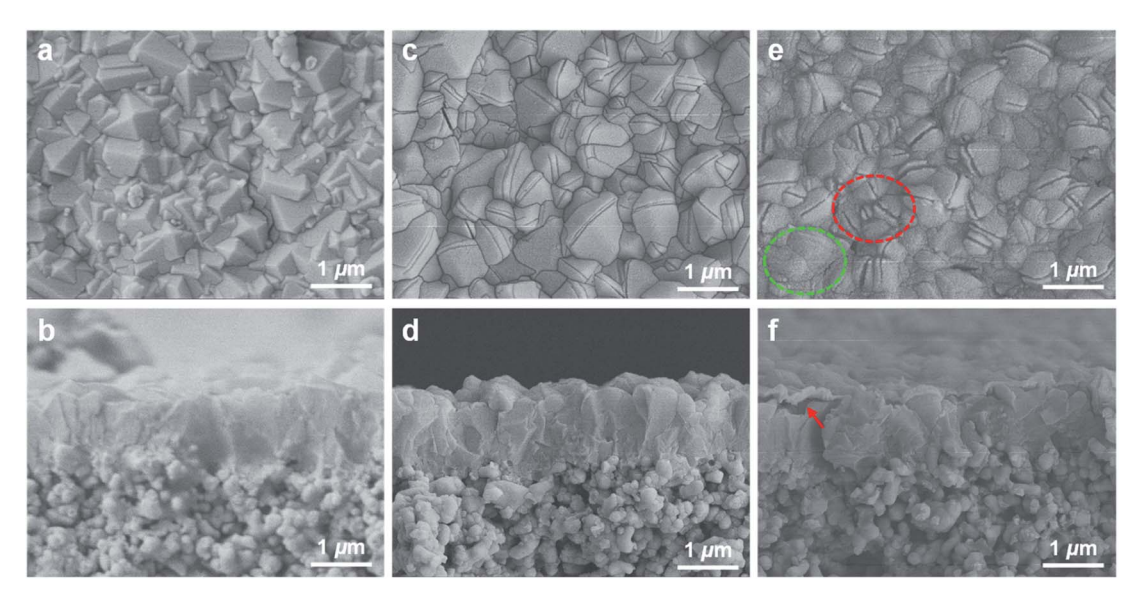


Fig. 3 SEM images of ZIF-8 (a and b), ZIF-8-BiB (c and d), and ZIF-8-PMMA (e and f) membranes. The green and red dotted circles in (e) indicate a region fully covered by PMMA and a region poorly covered by PMMA, respectively. The red arrow in (f) indicates the interfacial gap between PMMA and ZIF-8.

patterns were consistent with the simulated pattern, indicating the formation of crystalline ZIF-8 seeds and a ZIF-8 film without no identifiable impurities. According to the SEM images presented in Fig. S1,† the top surface of the α -alumina substrate was uniformly covered with ZIF-8 seed crystals of \sim 100 nm in size with some crystals inside the support, providing strong mechanical binding with the support.²⁴ After the secondary growth, the ZIF-8 seed layer was fully grown to a polycrystalline ZIF-8 membrane. The resulting ZIF-8 membrane was well intergrown with a thickness of \sim 1 µm (Fig. 3a and b).

As shown in Fig. 2, the PSLE of ZIF-8 membranes with his-BiB substantially lowered the (110) peak intensity, suggesting compromised crystallinity possibly due to partial degradation. It is known that harsh PSLE conditions can partially disintegrate MOFs since ligand exchange reactions are inherently destructive, involving dissolution, association, and even recrystallization in certain cases.21 For example, the PSLE of ZIF-8 by 2-imidazolecarboxaldehyde (Ica) generated cavities on ZIF-8 particles as well as on ZIF-8 membranes.18 The SEM images presented in Fig. 3c and d confirm this PSLE-induced partial degradation, revealing not only smoothening of grain surfaces but also formation of fissures on the (211) facets of the grains of the ZIF-8-BiB membrane. While the smoothened grain surfaces resulted from the surface restructuring, the fissure formation can be explained by the fact that more ligands were exchanged on the (211) planes than on other planes due to their higher metal-ligand bond density.25 As more his-BiB was incorporated on the (211) planes, the bulkier ligand induced tensile stress on the planes, thereby leading to the formation of fissures. Judging from the cross section of the membrane (Fig. 3d), the fissures seem to be limited to the top surface, not propagating through the grains. The effect of the surface restructuring and the (211) surface fissure formation is likely to reduce the effective membrane thickness without compromising the separation

capabilities of the membranes. It is noted that Cohen *et al.*²⁰ did not observe the formation of fissures on their ZIF-8 nanoparticles upon the PSLE of his-BiB possibly due to the relatively small fraction of the (211) surface termination of the truncated rhombic dodecahedral nanoparticles as compared to that of the current rhombic dodecahedral microparticles.

The fraction of the his-BiB ligand on a ZIF-8-BiB membrane was determined by 1 H NMR analysis. As the PSLE reaction time increased to 24 h, the his-BiB content increased linearly and saturated at \sim 1.2 mol% (Fig. S2†). The saturation concentration of the ZIF-8-BiB membrane was lower than that of the ZIF-8-BiB nanoparticles (\sim 2 mol%) by Cohen and coworkers, 20 likely due to the smaller surface-to-volume ratio of the ZIF-8 grains of the membranes than the nanoparticles (\sim 175 nm). The longer the PSLE reaction times (*i.e.*, 36 h and 48 h), the more membranes were disintegrated (Fig. S3†) though no significant changes were noticed in the XRD patterns (Fig. S4†). As such, the PSLE reaction time was set at 24 h.

Fig. 3e and f present the top and cross-sectional SEM images of a ZIF-8-PMMA membrane, respectively. A dense layer appeared on top of the polycrystalline ZIF-8 membrane (Fig. 3e and f). However, the PMMA layer exhibited surface defects (see the red circle in Fig. 3e) and separated from the underneath ZIF-8 layer (see the red arrow in Fig. 3f) possibly due to the weak interaction with certain regions of the ZIF-8 surfaces. The crystallinity of the ZIF-8-PMMA membrane was retained as evidenced by its well-defined diffraction pattern (Fig. 2). In fact, the ZIF-8-PMMA membrane showed a slightly higher (110) peak intensity than the ZIF-8-BiB membrane while exhibiting similar intensities of the other peaks, suggesting that the ATRP led to a reduction in the incoherent (110) diffraction caused by coordinated his-BiB ligands. Given its lower (110) peak intensity as compared to the ZIF-8 membrane, the effective thickness of the ZIF-8-PMMA membrane is expected to be still lower than that of the ZIF-8 membrane (Fig. 2). The lower effective thickness upon the PSSP process is expected to enhance the separation performance of the ZIF-8-PMMA membranes. The ATR FT-IR spectrum of the ZIF-8-PMMA membrane shows a peak at 1710 cm⁻¹ corresponding to carbonyl (i.e., C=O) stretching vibration, indicating the presence of a PMMA top layer (Fig. S6†), which is further confirmed by solution ¹H NMR performed by dissolving the ZIF-8-PMMA membrane (Fig. S7†). The amount of PMMA on the ZIF-8-PMMA membrane was estimated to be \sim 10.0 \pm 0.5 wt% (i.e., \sim 90.0 wt% ZIF-8) (Fig. S8†).

The morphology of the ZIF-8-PMMA membrane was further investigated by using the cross-sectional TEM images. The PMMA layer, which appears brighter (Fig. 4a), covered the darker ZIF-8 layer with a thickness of ~76 nm, in good agreement with SEM observation (Fig. 3f). Upon close examination, however, there appeared noticeable interfacial gaps present beneath the PMMA layer (see the red arrows in Fig. 4a), as observed in the SEM image (Fig. 3f). As indicated by the red circle in Fig. 4a, the PMMA layer was partially discontinuous. It implies that the 76 nm thick PMMA layer was not strongly bound to the ZIF-8 layer possibly due to the heterogeneity of the ZIF-8-BiB surfaces. As shown in the HRTEM image of an interfacial gap (Fig. 4b), however, a much thinner sub-10 nm thick amorphous PMMA layer (see a region and bottom left FFT diffraction) covered the surface of ZIF-8 (see b region and bottom right FFT diffraction). The sub-10 nm thick PMMA layer (hereafter surface PMMA layer) seemed to be different from the thicker PMMA layer (hereafter, PMMA overlayer). It was surmised that whereas the PMMA overlayer formed dominantly

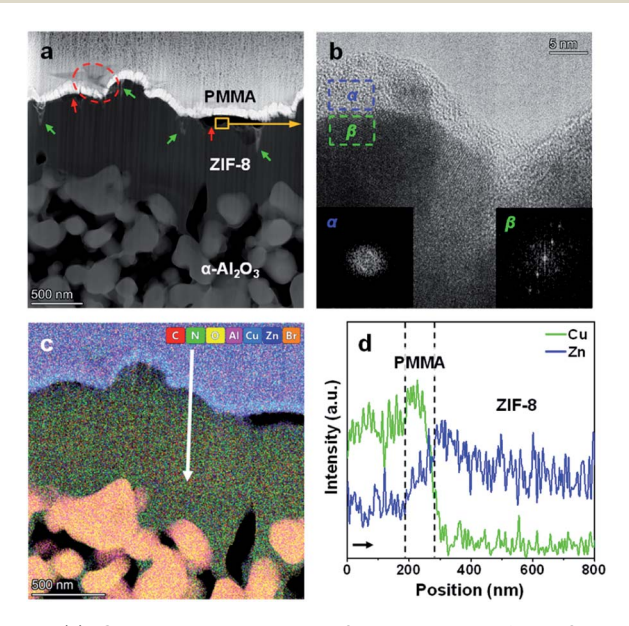


Fig. 4 (a) Cross-sectional HAADF-STEM images of ZIF-8-PMMA membranes. The red and green arrows in (a) indicate the interfacial gaps and the PMMA filled in the grain boundaries of the ZIF-8 layer, respectively. (b) HRTEM image of ZIF-8-PMMA membranes. The insets in (b) show FFT patterns from the designated regions. (c) EDX elemental mapping of the ZIF-8-PMMA membrane and (d) the corresponding elemental intensity along the arrow in (c). The dashed lines in (d) indicate the boundaries of PMMA.

by homogeneous polymerization, the surface PMMA layer might be polymerized heterogeneously from ZIF-8-BiB. It is noted that both homogeneous and heterogeneous polymerizations were initiated by the his-BiB of ZIF-8-BiB. As such, it is likely that these surface PMMA layers might seal grain boundary defects (see the green arrows in Fig. 4a).

Elemental analysis was conducted using TEM-EDX mapping. The PMMA layer was clearly distinguishable from the ZIF-8 layer (Fig. 4c and S9†). Interestingly, the elemental mapping exhibited a Cu signal in the PMMA layer (Fig. 4c and S9†). Linear scanning along the arrow in Fig. 4c revealed the relatively high intensity of the Cu signal only in the PMMA layer, while the Zn signal was clearly noticeable in the ZIF-8 layer (Fig. 4d). The Cu signal likely comes from the catalyst residue incorporated in the PMMA layer during the *in situ* polymerization process. It is known that catalysis residues are present in the polymers prepared by ATRP and efforts have been made to remove them.²⁶ In our case, however, the presence of Cu catalyst residue might be advantageous since both Cu⁺ and Cu²⁺ ions can enable facilitated transport for olefin molecules such as C₃H₆.²⁷ The oxidation states of the Cu residue were confirmed by XPS analysis. Fig. S10† shows the Cu 2p3/2 spectrum, which was deconvoluted to estimate \sim 40.7% of Cu^{2+} at 933.5 eV and 59.3% of Cu⁺ and Cu⁰ at 932.2 eV.²⁸

The C3 separation performances of ZIF-8, ZIF-8-BiB, and ZIF-8-PMMA membranes were tested and compared as presented in Fig. 5a and Table S1.† The ZIF-8 membranes showed a C₃H₆ permeance of $\sim 4.31 \times 10^{-8} \text{ mol m}^{-2} \text{ s}^{-1} \text{ Pa}^{-1}$ and a C_3H_6/C_3H_8 separation factor of ~60.1, which are within those reported in the literature. Upon PSLE, both the C₃H₆ permeance and C₃H₆/ C₃H₈ separation factor of the ZIF-8-BiB membranes decreased to $\sim 3.25 \times 10^{-8}$ mol m⁻² s⁻¹ Pa⁻¹ and ~ 44.4 , respectively (Fig. 5a). The decreased C₃H₆/C₃H₈ separation performance of the ZIF-8-BiB membranes might be attributed possibly to the partial pore blockage and the defects created upon the incorporation of the bulky his-BiB ligands.20 However, the ZIF-8-PMMA membranes showed an increase both in their C₃H₆ permeance ($\sim 5.58 \times 10^{-8} \text{ mol m}^{-2} \text{ s}^{-1} \text{ Pa}^{-1}$) and C_3H_6/C_3H_8 separation factor (\sim 105.5) by \sim 30% and \sim 76%, respectively, as compared to the ZIF-8 membranes (Fig. 5a). The enhanced separation factor of the ZIF-8-PMMA membranes was likely due to the effective sealing of grain boundary defects and the possible facilitated transport of C₃H₆ by Cu ions in the PMMA layer. However, the increased C₃H₆ permeance of the ZIF-8-PMMA membranes was somewhat unexpected. This unexpected increase of the C₃H₆ permeance of the ZIF-8-PMMA membranes could be attributed mostly to the reduced effective thickness (see Fig. 2). To some extent, the facilitated transport by Cu ions in the exceptionally thin sub-10 nm thick surface PMMA layers might have contributed to the permeance increase as well. Given the very low gas permeability of typical dense PMMA29 and the surface defects on the PMMA overlayers (see the red circles in Fig. 3e and 4b), it is likely that the thicker PMMA overlayers had little effects on the separation properties of the ZIF-8-PMMA membranes. Besides, the ultra-thin PMMA layer on the ZIF-8 layer might likely exhibit different microstructures (i.e., free volume) due to different chain mobility and

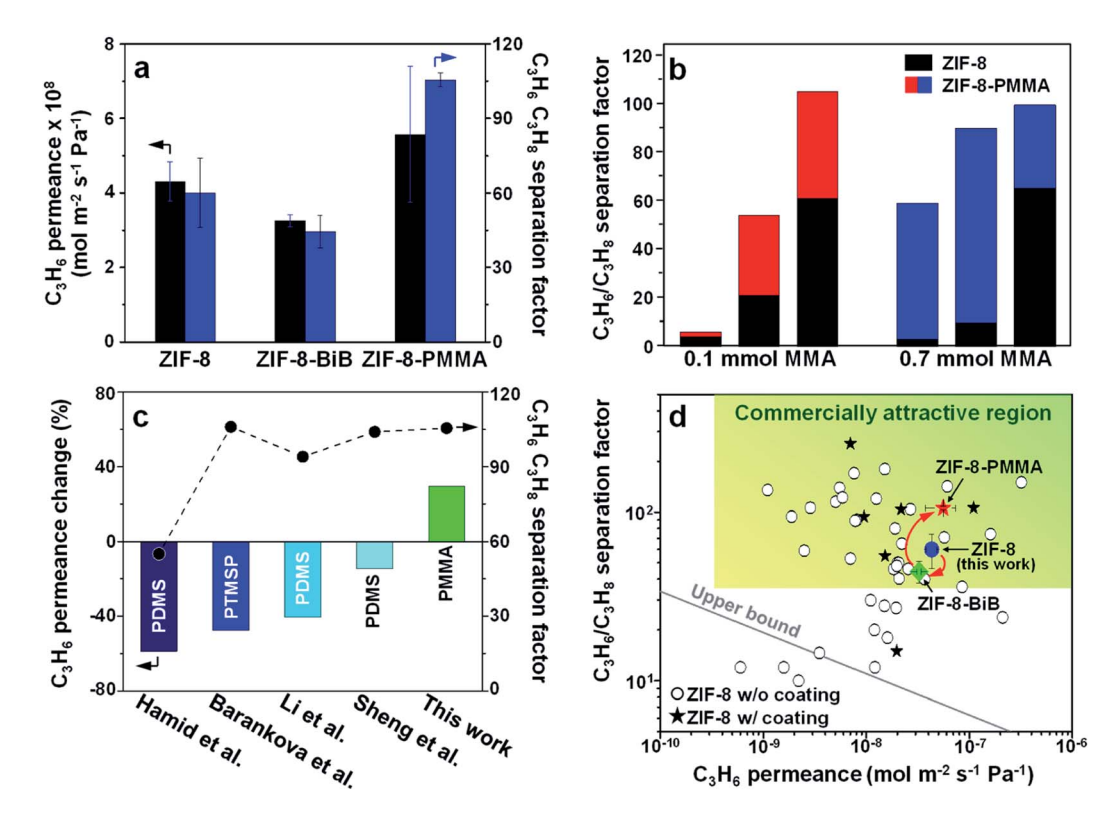


Fig. 5 (a) C_3H_6 permeabilities and C_3H_6/C_3H_8 separation factors of ZIF-8, ZIF-8-BiB, and ZIF-8-PMMA membranes. (b) Effect of MMA contents on the C₃H₆/C₃H₈ separation factor improvements of ZIF-8 membranes with various grain boundary defects. (c) Effect of different polymer coatings on the C_3H_6/C_3H_8 separation performances of ZIF-8 membranes. The left y-axis indicates percentage changes in the C_3H_6 permeances upon polymer coating. (d) C_3H_6/C_3H_8 separation performances of ZIF-8, ZIF-8-BiB, and ZIF-8-PMMA membranes in comparison with the reported ZIF-8 membranes.^{6-10,20,25,32-50} The commercially attractive region and the polymeric upper bound in (d) were marked based on a membrane thickness of 1 μ m. ^{51,52}

high packing density resulting from its interaction with solid surfaces,30 thereby showing enhanced gas diffusion rates as compared with its bulk counterpart.

To investigate the effectiveness of the PSSP strategy, the strategy was applied to ZIF-8 membranes with various grain boundary defects (Fig. 5b and Table S2†). As shown in Fig. 5b, at a low MMA monomer concentration (0.1 M), major improvements by the PSSP were made only for those ZIF-8 membranes with separation factors greater than \sim 20 (Fig. 5b). This is likely due to the inadequate defect sealing of more pronounced defects (i.e., bigger grain boundary defects) of the poorly intergrown ZIF-8 membranes resulting from insufficient PMMA. With increased MMA monomer concentrations (0.7 M) (Fig. S11†), 23 significant enhancements were shown even for the poorly intergrown ZIF-8 membranes (i.e., from \sim 3 to \sim 60 and from \sim 10 to \sim 91) (Fig. 5b).

Finally, the PSSP process was compared with conventional polymer solution processing methods using highly permeable polymers such as PDMS and PTMSP. After coating, most of the ZIF-8 membranes showed much improved C₃H₆/C₃H₈ separation factors (Fig. 5c). While the C₃H₆ permeances of the ZIF-8-PDMS and ZIF-8-PTMSP membranes decreased substantially; however, ZIF-8-PMMA showed improved C₃H₆ permeances (Fig. 5c) as explained above. The ZIF-8-PMMA membranes compare well with other high-performance

membranes,7-11,24,31-50 proving the effectiveness of the PSSP process (Fig. 5d).51,52 It is worth noting that when coated by conventional methods such as slip coating, the PMMA layer is expected to significantly decrease the gas permeance of the ZIF-8 membranes due to the inherently low permeability of bulk PMMA and the relatively greater thickness. Furthermore, the C3 separation performance of the ZIF-8-PMMA membranes was found quite stable over time (Fig. S12†).

Experimental

Materials

Histamine dihydrochloride (>99%), α-bromoisobutyryl bromide (BiBB, 98%), methyl methacrylate (MMA, 99%), magnesium sulfate (>97%), copper(II) chloride (99.999%) N,N,N',N",N"pentamethyldiethylenetriamine (PMDTA, 99%), ascorbic acid (AA, Pharmaceutical Secondary Standard), zinc nitrate hexahydrate (98%), 2-methylimidazole (2-mIm, 99%), and sodium formate (>99%) were purchased from Sigma Aldrich. Other chemical reagents and solvents including triethylamine (TEA, 99%, Alpha Aesar), dichloromethane (DCM, >99.5%, Alfa Aesar), methanol (MeOH, >99.8%, Alfa Aesar), chloroform (99.8%, VWR Chemicals BDH®), potassium hydroxide (KOH, >85%, VWR Chemicals BDH®), ethyl acetate (EtOAc, >99.5%, VWR Chemicals BDH®), toluene (>99.5%, VWR Chemicals BDH®), and 1-butanol (>99.4%, J. T. Baker®) were used as received.

Synthesis of N-(2-(1H-imidazole-4-yl)ethyl)-2-bromo-2methylpropanamide (his-BiB)

The synthesis procedure of his-BiB was described elsewhere.20 Briefly, 5.0 g of histamine dihydrochloride was added to a mixture of chloroform (400 ml) and TEA (12.7 g) in a 1 L round bottle flask. After fully dissolving histamine dihydrochloride, 12.7 g of BiBB was added into the solution dropwise using a syringe at 0 °C. Then the mixture underwent a reaction at room temperature for 12 h. The solution became transparent and brownish. After that, the reacted solution was quenched to deactivate unreacted reagents by pouring an aqueous KOH solution (106 g of KOH in 450 ml of H2O) into the solution under vigorous shaking. The bottom solution (chloroform/his-BiB) was decanted using a funnel. This quenching/decanting process was repeated three times. To increase the yield, his-BiB in the used KOH solution was retrieved by thoroughly washing with dichloromethane (DCM) several times. Again, the his-BiB/DCM solution was separated using a funnel. The solvents (i.e., chloroform and DCM) were evaporated at 40 °C overnight. The as-synthesized his-BiB precipitates were redissolved in a small amount of MeOH and recrystallized with EtOAc and dried at 40 °C for one day. A yellowish his-BiB powder was obtained. The yield of his-BiB was 76%, which was comparable with the yield reported.20

Synthesis of ZIF-8 membranes

Polycrystalline ZIF-8 membranes were prepared via microwaveassisted seeding and subsequent secondary growth on porous α-alumina disks (2.2 cm in diameter) as previously reported.³⁷ The alumina disks were prepared following the procedure described in our previous work.53 For microwave seeding, a metal precursor solution (2.43 g of zinc nitrate hexahydrate dissolved in 40 ml of MeOH) and a ligand precursor solution (2.59 g of 2-mIm and 0.125 g of sodium formate dissolved in 30 ml of MeOH) were prepared separately. An α-alumina disk was placed vertically in a custom-made Teflon holder and immersed in the metal precursor solution at room temperature for an hour. The saturated α-alumina disk with the metal solution was then placed into a microwave-transparent glass tube containing the ligand precursor solution and immediately subjected to microwave irradiation with 100 W for 1.5 min. After resting inside the microwave oven (CEM, Discover-SP w/ ActiVent®) for 30 min, the ZIF-8 seeded α-alumina disk was washed in MeOH on a lab shaker for 12 h. The ZIF-8 seed layer was dried at 60 °C for 4 h. For the secondary growth, a metal precursor solution (0.11 g of zinc nitrate hexahydrate dissolved in 20 ml of DI water) and a ligand precursor solution (2.27 g of 2mIm dissolved in 18 ml of DI water) were prepared separately. The metal precursor solution was poured into the ligand precursor solution and stirred with a magnetic bar for 2 min. The seeded disk was placed vertically in a custom-made Teflon holder and immersed in the mixed solution in a beaker. After covering with a parafilm, the beaker was placed in a convection

oven at 30 $^{\circ}$ C for 6 h. The resulting ZIF-8 membrane sample was washed in MeOH on a lab shaker at room temperature for 1 d and dried under the atmosphere for 12 h.

Post-synthetic ligand exchange (PSLE) of ZIF-8 membranes with BiB

A 0.025 M his-BiB stock solution was prepared by dissolving 5.2 g of his-BiB powder in 800 ml of 1-butanol. 0.1 g of TEA was added to 12 ml of the his-BiB solution to adjust the pH to \sim 7, which was necessary to prevent undesirable degradation of the ZIF-8 membrane in the his-BiB solution. A ZIF-8 membrane was placed vertically in a custom-made Teflon holder and put into an autoclave containing the his-BiB/TEA solution. The autoclave was placed in a convection oven at 40 °C for 24 h. The resulting membrane (hereafter, ZIF-8-BiB membrane) was washed with MeOH overnight and dried under the atmosphere.

Atom transfer radical polymerization (ATRP) of ZIF-8-BiB membranes

In a typical synthesis, a ZIF-8-BiB membrane was inserted vertically in a Teflon holder and placed in a heavy wall glass tube. 12 ml of MeOH was poured into the glass tube until the membrane is completely immersed. 13.8 mg of MMA purified was mixed with 0.5 ml of MeOH. The solution mixture was added to the glass tube under magnetic stirring. After that, 0.2 ml of a CuCl₂/PMDETA stock solution was added. The stock solution was prepared by adding 85.5 mg of PMDETA and 5.5 mg of CuCl₂ sequentially in 200 ml of MeOH. The glass tube was sealed and the solution was degassed with several freepump-thaw cycles in a vacuum line. 0.17 mg of AA was dissolved in 0.2 ml of MeOH and the AA solution was degassed. The degassed AA solution was added into the glass tube dropwise. The ATRP reaction was continued for 18 h at room temperature. After that, the resulting ZIF-8-PMMA membrane was sequentially washed in MeOH for 12 h and subsequently in toluene for another 12 h and dried under atmospheric conditions overnight.

Characterization

Powder X-ray diffraction (PXRD) patterns were obtained using an X-ray diffractometer (Rigaku Miniflex II) in a 2θ range from 5° to 30° with Cu-K α radiation ($\lambda = 1.5406$ Å). Electron micrographs were taken using a field-emission scanning electron microscope (FE-SEM, JEOL JSM-7500F) at a working distance of 15 mm and acceleration voltage of 5 keV. Vibrational spectra were recorded using an attenuated total reflectance Fourier transform infrared (ATR-FTIR) spectrometer (Thermo Scientific Nicolet iS5 equipped with an iD7 ATR) at the range of 4000 to 400 cm⁻¹ with a resolution of 4 cm⁻¹. Solution proton nuclear magnetic resonance (¹H NMR) spectra were obtained using a Bruker Avance III (400 MHz system). NMR samples were prepared by dissolving his-BiB in 600 μL of CD₃OD-d₄ and ZIF-8 and ZIF-8-BiB membrane samples in 20 µL of D₂SO₄-d₂ mixed with 580 μL of CD₃OD-d₄. Thermogravimetric analysis (TGA) was carried out using a Q50 (TA instruments) in the temperature range of 25-800 °C with a ramp rate of 10 °C min⁻¹ under

an air flow of 50 cm³ min⁻¹. For TEM imaging and analysis, membrane samples were etched using a Tescan LYRA-3 Model GMH dual-beam FIB instrument. TEM imaging and analysis were conducted by using a FEI Tecnai G2 F20 Super-Twin FE-TEM operating at 120 kV. X-ray photoelectron spectra (XPS) were obtained using an Omicron ESCA+ with a Mg X-ray source at 300 W.

Gas permeation measurements

The binary propylene/propane 50/50 separation performances of the membranes were measured using the Wicke–Kallenbach technique at room temperature under atmospheric pressure. The total gas flow rate on the feed side was 100 cm³ min⁻¹ while the permeate side was swept by flowing argon at 100 cm³ min⁻¹. The composition of the permeate was analyzed using a gas chromatograph (GC 7890A, Agilent) equipped with a flame ionized detector (FID) and a HP-plot Q column.

Conclusions

In conclusion, we have successfully demonstrated a new defect sealing strategy, post-synthetic surface polymerization (PSSP), consisting of post-synthetic ligand exchange (PSLE) and subsequent atom transfer radical polymerization (ATRP). The in situ polymerization of poly(methyl methacrylate) (PMMA) on top of his-BiB-exchanged ZIF-8 membranes led to the formation of ultra-thin sub-10 nm PMMA layers covering the ZIF-8 surfaces and sealing the grain boundary defects. The PSSP resulted in ZIF-8-PMMA membranes with significantly increased C₃H₆/ C_3H_8 separation factors (i.e., from 60.1 \pm 13.9 to 105.5 \pm 2.8) and unexpectedly enhanced C_3H_6 permeances (i.e., from 4.31 \pm 0.53×10^{-8} to $5.58 \pm 1.82 \times 10^{-8}$ mol m⁻² s⁻¹ Pa⁻¹), outperforming the conventional polymer solution processing methods. These unexpected results were attributed possibly to (1) the effective grain boundary defect healing, (2) the reduced effective thickness by partial degradation upon the PSSP process, and (3) the possible facilitated transport of C₃H₆ by Cu ions in the sub-10 nm thick PMMA layers. The new strategy presented here is expected to substantially lower the cost of the membranes due not only to the substantially improved membrane performances but also to the enhanced reproducibility, thereby bringing polycrystalline MOF membranes close to their practical applications.

Conflicts of interest

There are no conflicts to declare.

Acknowledgements

H.-K. J. acknowledges the financial support from the National Science Foundation (CBET-1929596). This publication was made possible in part by NPRP grant #12S-0209-190064 from the Qatar National Research Fund (a member of Qatar Foundation). The findings presented herein are solely the responsibility of the authors. The National Science Foundation

supported the FE-SEM acquisition under grant DBI-0116835, the VP for Research Office, and the Texas A&M Engineering Experimental Station. The authors would like to thank Mr Yuji Katayama of Asahi Kasei Corporation for his valuable comments on ligand synthesis.

References

- 1 K. S. Park, Z. Ni, A. P. Cote, J. Y. Choi, R. D. Huang, F. J. Uribe-Romo, H. K. Chae, M. O'Keeffe and O. M. Yaghi, *Proc. Natl. Acad. Sci. U. S. A.*, 2006, **103**, 10186–10191.
- C. Zhang, R. P. Lively, K. Zhang, J. R. Johnson, O. Karvan and W. J. Koros, *J. Phys. Chem. Lett.*, 2012, 3, 2130–2134.
- 3 Z. P. Lai, Curr. Opin. Chem. Eng., 2018, 20, 78-85.
- 4 M. R. A. Hamid and H. K. Jeong, *Korean J. Chem. Eng.*, 2018, 35, 1577–1600.
- 5 D. Korelskiy, P. Ye, M. S. Nabavi and J. Hedlund, *J. Mater. Chem. A*, 2017, 5, 7295–7299.
- 6 Q. Q. Hou, S. Zhou, Y. Y. Wei, J. Caro and H. H. Wang, *J. Am. Chem. Soc.*, 2020, 142, 9582–9586.
- 7 M. R. A. Hamid and H. K. Jeong, *J. Ind. Eng. Chem.*, 2020, **88**, 319–327.
- 8 M. R. A. Hamid, S. Park, J. S. Kim, Y. M. Lee and H. K. Jeong, *Ind. Eng. Chem. Res.*, 2019, **58**, 14947–14953.
- 9 J. F. Li, H. Q. Lian, K. F. Wei, E. Y. Song, Y. C. Pan and W. H. Xing, *J. Membr. Sci.*, 2020, **595**, 117503–117510.
- 10 L. Q. Sheng, C. Q. Wang, F. Yang, L. Xiang, X. J. Huang, J. Yu, L. X. Zhang, Y. C. Pan and Y. S. Li, *Chem. Commun.*, 2017, 53, 7760–7763.
- 11 E. Barankova, X. Tan, L. F. Villalobos, E. Litwiller and K. V. Peinemann, *Angew. Chem., Int. Ed.*, 2017, **56**, 2965–2968.
- 12 S. Friebe, B. Geppert, F. Steinbach and J. Caro, ACS Appl. Mater. Interfaces, 2017, 9, 12878–12885.
- 13 D. E. Sanders, Z. P. Smith, R. L. Guo, L. M. Robeson, J. E. McGrath, D. R. Paul and B. D. Freeman, *Polymer*, 2013, 54, 4729–4761.
- Karagiaridi, W. Bury, A. A. Sarjeant, C. L. Stern,
 K. Farha and J. T. Hupp, *Chem. Sci.*, 2012, 3, 3256–3260.
- H. F. Zhang, J. James, M. Zhao, Y. Yao, Y. S. Zhang,
 B. Q. Zhang and Y. S. Lin, J. Membr. Sci., 2017, 532, 1–8.
- 16 M. Kim, J. F. Cahill, Y. X. Su, K. A. Prather and S. M. Cohen, *Chem. Sci.*, 2012, 3, 126–130.
- 17 W. B. Li, Y. F. Zhang, C. Y. Zhang, Q. Meng, Z. H. Xu, P. C. Su, Q. B. Li, C. Shen, Z. Fan, L. Qin and G. L. Zhang, *Nat. Commun.*, 2016, 7, 11315–11324.
- 18 M. J. Lee, H. T. Kwon and H. K. Jeong, Angew. Chem., Int. Ed., 2018, 57, 156–161.
- O. Karagiaridi, M. B. Lalonde, W. Bury, A. A. Sarjeant,
 O. K. Farha and J. T. Hupp, J. Am. Chem. Soc., 2012, 134, 18790–18796.
- 20 Y. Katayama, M. Kalaj, K. S. Barcus and S. M. Cohen, J. Am. Chem. Soc., 2019, 141, 20000–20003.
- 21 K. C. Jayachandrababu, D. S. Sholl and S. Nair, *J. Am. Chem. Soc.*, 2017, **139**, 5906–5915.
- 22 Y. H. Zhu, J. Ciston, B. Zheng, X. H. Miao, C. Czarnik, Y. C. Pan, R. Sougrat, Z. P. Lai, C. E. Hsiung, K. X. Yao, I. Pinnau, M. Pan and Y. Han, *Nat. Mater.*, 2017, 16, 532.

- 23 K. Xie, Q. Fu, C. L. Xu, H. Lu, Q. H. Zhao, R. Curtain, D. Y. Gu, P. A. Webley and G. G. Qiao, Energy Environ. Sci., 2018, 11, 544-550.
- 24 H. T. Kwon and H. K. Jeong, J. Am. Chem. Soc., 2013, 135, 10763-10768.
- 25 O. M. Linder-Patton, T. J. de Prinse, S. Furukawa, S. G. Bell, K. Sumida, C. J. Doonan and C. J. Sumby, Crystengcomm, 2018, 20, 4926-4934.
- 26 Y. Q. Shen, H. D. Tang and S. J. Ding, Prog. Polym. Sci., 2004, 29, 1053-1078.
- 27 G. H. Hsiue and J. S. Yang, Macromol. Symp., 1996, 105, 51-
- 28 C. K. Wu, M. Yin, S. O'Brien and J. T. Koberstein, Chem. Mater., 2006, 18, 6054-6058.
- 29 Y. Nakai, H. Yoshimizu and Y. Tsujita, Polym. I., 2006, 38, 376-380.
- 30 C. J. Ellison and J. M. Torkelson, Nat. Mater., 2003, 2, 695-700.
- 31 S. Tanaka, K. Okubo, K. Kida, M. Sugita and T. Takewaki, J. Membr. Sci., 2017, 544, 306-311.
- 32 A. J. Brown, N. A. Brunelli, K. Eum, F. Rashidi, J. R. Johnson, W. J. Koros, C. W. Jones and S. Nair, Science, 2014, 345, 72-75.
- 33 K. Eum, A. Rownaghi, D. Choi, R. R. Bhave, C. W. Jones and S. Nair, Adv. Funct. Mater., 2016, 26, 5011-5018.
- 34 K. Eum, C. Ma, A. Rownaghi, C. W. Jones and S. Nair, ACS Appl. Mater. Interfaces, 2016, 8, 25337-25342.
- 35 N. Hara, M. Yoshimune, H. Negishi, K. Haraya, S. Hara and T. Yamaguchi, J. Membr. Sci., 2014, 450, 215-223.
- 36 X. Jiang, S. W. Li, Y. P. Bai and L. Shao, J. Mater. Chem. A, 2019, 7, 10898-10904.
- 37 H. T. Kwon and H. K. Jeong, Chem. Commun., 2013, 49, 3854-3856.
- 38 M. J. Lee, M. R. A. Hamid, J. Lee, J. S. Kim, Y. M. Lee and H. K. Jeong, J. Membr. Sci., 2018, 559, 28-34.

- 39 D. F. Liu, X. L. Ma, H. X. Xi and Y. S. Lin, J. Membr. Sci., 2014, 451, 85-93,
- 40 X. L. Ma, P. Kumar, N. Mittal, A. Khlyustova, P. Daoutidis, K. A. Mkhoyan and M. Tsapatsis, Science, 2018, 361, 1008-
- 41 Y. C. Pan, T. Li, G. Lestari and Z. P. Lai, J. Membr. Sci., 2012, **390.** 93-98.
- 42 Y. C. Pan, W. Liu, Y. J. Zhao, C. Q. Wang and Z. P. Lai, J. Membr. Sci., 2015, 493, 88-96.
- 43 G. Ramu, M. Lee and H. K. Jeong, Microporous Mesoporous Mater., 2018, 259, 155-162.
- 44 E. Shamsaei, X. C. Lin, Z. X. Low, Z. Abbasi, Y. X. Hu, J. Z. Liu and H. T. Wang, ACS Appl. Mater. Interfaces, 2016, 8, 6236-6244.
- 45 N. T. Tran, J. Kim and M. R. Othman, Microporous Mesoporous Mater., 2019, 285, 178-184.
- 46 N. T. Tran, T. Yu, J. Kim and M. R. Othman, Sep. Purif. Technol., 2020, 251, 117354-117360.
- 47 R. C. Wei, H. Y. Chi, X. Li, D. W. Lu, Y. Wan, C. W. Yang and Z. P. Lai, Adv. Funct. Mater., 2020, 30, 1907089-1907095.
- 48 J. Yu, Y. C. Pan, C. Q. Wang and Z. P. Lai, Chem. Eng. Sci., 2016, 141, 119-124.
- 49 H. T. Kwon, H. K. Jeong, A. S. Lee, H. S. An, T. Lee, E. Jang, J. S. Lee and J. Choi, Chem. Commun., 2016, 52, 11669-11672.
- 50 M. Hayashi, D. N. T. Lee, M. D. de Mello, J. A. Boscoboinik and M. Tsapatsis, Angew. Chem., Int. Ed., 2021, 133, 9402-9406.
- 51 C. Colling, G. Huff and J. Bartels, US Pat., US 20040004040A1, 2002.
- 52 R. L. Burns and W. J. Koros, J. Membr. Sci., 2003, 211, 299-
- 53 S. Park and H.-K. Jeong, J. Mater. Chem. A, 2020, 8, 23645-23653.